Available online at www.sciencedirect.com
SCIENCE DIRECT®
Thermochimica Acta 430 (2005) 201–210
thermochimica acta
www.elsevier.com/locate/tca

On the kinetics of melting and crystallization of poly(L-lactic acid) by TMDSC

M. Salmerón Sánchez [a,*], J.L. Gómez Ribelles [a], F. Hernández Sánchez [b], J.F. Mano [c,d]

[a] *Center for Biomaterials, Universidad Politécnica de Valencia, Camino de Vera s/n, 46022 Valencia, Spain*
[b] *Centro de Investigaciones Científicas del Yucatán, C.43 No. 130, Chuburná de Hidalgo, CP 97200 Mérida, Mexico*
[c] *Polymer Engineering Department, University of Minho, Campus of Azurém, 4800-058 Guimarães, Portugal*
[d] *3B's Research Group, Biomaterials, Biodegradables and Biomimetics, University of Minho, 4710-057 Braga, Portugal*

Received 22 November 2004; received in revised form 27 January 2005; accepted 29 January 2005
Available online 2 March 2005

Abstract

The crystallization and melting process of poly(L-lactic acid), PLLA, is investigated by temperature modulated differential scanning calorimetry, TMDSC. The sample is cooled from the melt to different temperatures and the crystallization process is followed by subjecting the material to a modulated quasi-isothermal stage. From the average component of the heat flow and the application of the Lauritzen–Hoffman theory two crystallization regimes are identified with a transition temperature around 118 °C. Besides, the oscillating heat flow allows calculating the crystal growth rate via the model proposed by Toda et al., what gives, in addition, an independent determination of the transition temperature from modulated experiments. Further, the kinetics of melting is studied by modulated heating scans at different frequencies. A strong frequency dependence is found both in the real and imaginary part of the complex heat capacity in the transition region. The kinetic response of the material to the temperature modulation is analyzed with the model proposed by Toda et al. Finally, step-wise quasi-isothermal TMDSC was used to investigate the reversible surface crystallization and melting both on cooling and heating and a small excess heat capacity is observed.

Keywords: TMDSC; PLLA; Melting; Crystallization; Kinetics

1. Introduction

Poly(L-lactic acid), PLLA, is a well known biodegradable and biocompatible polymer that has been widely used in many biomedical applications [1–3] such as wound closure, prosthetic implants, controlled-released systems and three-dimensional scaffolds. PLLA degradation takes place via hydrolysis whose rate depends strongly on crystalline and lamellar organization in the material [4,5]. The thermal history influences the crystallinity and microstructure of the material and the knowledge of the kinetics of the process becomes fundamental for the control of the morphology and therefore of the degradation rates required at each application [6,7]. In this way, the cooling rate strongly influences the degree of crystallinity of the system even when the material is isothermally crystallized, i.e. crystallization temperature determines the morphology of the crystals. It is known that both the nucleation rate J and the growth rate G depend non-monotonically upon the extent of supercooling (the discussion could be extended if heterogeneous and homogeneous nucleation is analyzed independently. In the case of a heterogeneous nucleation process an increasing cumulative function of nuclei with decreasing temperature would make more sense) and, besides, the maximum of J is at lower temperature than that of G [8]. At low temperatures, the reduced molecular mobility enhances the nucleation rate compared to the crystal growth rate, leading to the formation of a high number of small crystals. On the other hand, at low degrees of supercooling, crystal growth is faster than

* Corresponding author. Tel.: +34 963877275; fax: +34 963877276.
E-mail address: masalsan@fis.upv.es (M. Salmerón Sánchez).

0040-6031/$ – see front matter © 2005 Elsevier B.V. All rights reserved.
doi:10.1016/j.tca.2005.01.066

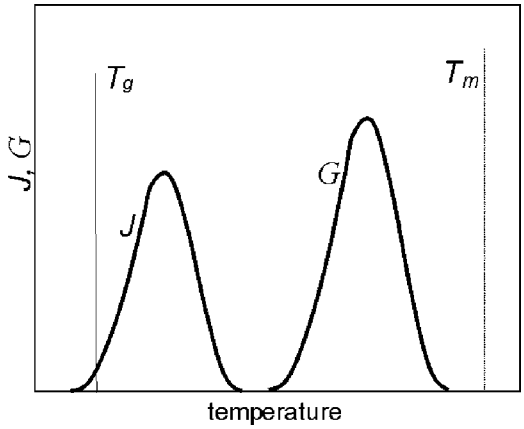

Fig. 1. Sketch of the crystal growth rate G and the nucleation rate J. G is localized at higher temperatures than G.

nucleation leading to the formation of a lower number of bigger crystals. A sketch of J and G is shown in Fig. 1. The position of the two curves shows the particular situation in which nuclei are formed on cooling and crystal growth is able to take place on the subsequent heating scan.

Temperature modulated differential scanning calorimetry, TMDSC, has been extensively used for studying the melting and crystallization phenomena in polymer systems (see [9] and references therein) and it is widely accepted that it can supply additional information compared to conventional DSC. In TMDSC the conventional DSC temperature program is superimposed with a dynamic temperature change. Due to the phase lag, φ, between the calorimeter response function (i.e. the heat flow) and the time derivative of the modulated temperature program, a complex apparent heat capacity, C^*, is defined whose modulus is

$$|C^*| = \frac{\dot{Q}_a}{\omega T_a}. \tag{1}$$

Here $\dot{Q}_a$ is the amplitude of the oscillating heat flow (or the first harmonic of the periodic component of the heat flow in the usual case the profile is not sinusoidal), T_a is the amplitude of the temperature wave, and ω is the modulation frequency. Since data treatment is done through a Fourier analysis a linear response of the process is assumed, i.e. in the case a sinusoidal temperature modulation is programmed a pure sinusoidal response should be obtained in the heat flow. In this way, selecting the adequate combinations of values of underlying heating rate, frequency and temperature amplitude, three temperature dependent magnitudes are obtained as representatives of a TMDSC experiment [10–12]:

$$C_\beta = \frac{\dot{Q}_u}{\beta}, \tag{2a}$$

$$C' = |C^*|\cos\varphi, \tag{2b}$$

$$C'' = |C^*|\sin\varphi. \tag{2c}$$

Eq. (2a) describes the heating rate dependent heat capacity obtained from the underlying component of the heat flow, $\dot{Q}_u$, i.e. the frequency independent component in the Fourier analysis, and is equivalent to the trace of a conventional DSC analysis at the average heating rate, β. Eq. (2b) gives the real part of the complex heat capacity, the component in phase with the heat flow, and Eq. (2c) the imaginary part, the out of phase component that appears when time dependent processes take place in the sample.

In this work we have used TMDSC for gain a better insight in the kinetics of crystallization and melting of PLLA. We show that TMDSC is able to provide from a single set of quasi-isothermally crystallization curves, on the one hand, a regime analysis of the crystal growth kinetics via the Lauritzen–Hoffmann theory [13,14] and, on the other hand, a direct estimation of the crystal growth rate via the method developed by Toda et al. [15,16]. Besides, the transition between the crystallization regimes is obtained in an independent way both from the underlying heat flow and the modulated experiments.

Melting of polymer crystals is a complicated phenomenon since there is usually a distribution of non-equilibrium melting points [17] which gives rise to a broad endothermic peak in a DSC scan. However, it is known that melting is a fast process that takes place with small superheating and it is likely that a fraction of crystals having melting points slightly lower than sample temperature melts in a time interval comparable to the temperature modulation period, and so a frequency response in a TMDSC experiment is expected. This frequency dependence is exploited through the kinetic modelling of melting due to Toda et al. and related to the temperature dependence of the melting rate coefficient [18–21].

Finally, polymer crystallites are said to be metastable, i.e. they are able to melt below the equilibrium melting point while crystal growth is still possible, and the melting process is said to be reversible in the sense that if the material is subjected to a modulated amplitude around a constant temperature, the thermal response is recovered in one period of the modulated temperature [22]. This phenomenon, already studied in other polymer systems [9,23] is studied for PLLA in this work.

2. Experimental

2.1. Material

PLLA was synthesised by classical polycondensation procedures. The polymerization reactions were carried out as described elsewhere [24]. Briefly, a glass polymerization reactor equipped with a nitrogen flow-through inlet and a vacuum connection, was placed in a temperature-controlled bath containing silicone oil. Polymerization was performed under nitrogen atmosphere at the temperature range of 100–150 °C for 12–48 h. In order to remove residual monomers, chloroform and methanol were used as the solvent and precipitant, respectively. The molecular weights of the polymer, M_n and M_w, were 58,000 and 132,000,

respectively, evaluated from gel permeation chromatography (Shimadzu, LC 10A, Japan) using polystyrene as standard and chloroform as solvent. Samples of around 2 mg were encapsulated in DSC pans for solids what provides a good contact between sample and pan and cover. Due to the thermal degradation of PLLA at high temperatures, each sample was used for no more than three DSC scans.

2.2. Apparatus

TMDSC was performed in a Pyris 1 apparatus (Perkin Elmer). Dry nitrogen gas was let through the DSC cell with a flow rate of 20 ml/min. The temperature of the equipment was calibrated by using indium and benzene. The heat of fusion of indium was used for calibrating the heat flow.

2.3. Temperature programs

Modulated quasi-isothermal crystallization was performed at different temperatures T_c between 70 and 140 °C starting from the melt and cooling at 100 °C/min to the desired temperature. An saw-tooth oscillating temperature profile was superimposed at each temperature T_c with amplitude 0.1 °C and period 24 s.

Melting kinetics was studied after erasing the thermal history of the sample at temperatures above the melting point for several minutes. Afterwards, the sample was subjected to a cooling scan from the melt at a rate of 40 °C/min, what allows a good cooling control and, therefore, the same thermal history in each sample. No crystallization event was detected during the cooling scan for this polymer, i.e. crystallization took place during the subsequent heating scan. The modulated temperature program was a tooth-saw temperature profile with an average heating rate of 1.5 °C/min, 0.1 °C of amplitude and different modulation periods, P (48, 60, 78, 84 s). A modulated empty pan curve with the same conditions was performed immediately after each scan and was later subtracted from the measured oscillating heat flow in order to obtain the TMDSC parameters. The temperature programs were selected so as to comply with a heating condition always, i.e.,

$$\frac{dT_s}{dt} > 0. \tag{3}$$

This is achieved in the equipment used in this work selecting the adequate input parameters that define the temperature cycle (T_1, T_2, T_3 and β_1), taking into account that

$$T_s(t) = \begin{cases} T_1 + \beta_1 t & \text{for } 0 \le t \le \frac{P}{2}, \\ (2T_2 - T_3) + \frac{T_3 - T_2}{T_2 - T_1}\beta_1 t & \text{for } \frac{P}{2} \le t \le P, \end{cases} \tag{4a}$$

$$\beta = \frac{\beta_1(T_3 - T_1)}{2(T_2 - T_1)}, \tag{4b}$$

$$T_a = \frac{1}{2}\left(T_2 - \frac{T_1 + T_3}{2}\right), \tag{4c}$$

$$P = \frac{2(T_2 - T_1)}{\beta_1}. \tag{4d}$$

Step-wise quasi-isothermal experiments were performed both on cooling and heating with a temperature step of 5 °C followed by an isothermal waiting time of 60 min in which the sample was subjected to a tooth-saw temperature profile, 0.1 °C amplitude and 24 s modulation period.

3. Results and discussion

Fig. 2a–c shows the underlying component of the heat flow as a function of time at each one of the crystallization temperatures T_c. Crystallization was absent at temperatures below 90 °C and above 140 °C, within the available experimental time scale. It is clearly shown than the minimum of the crystallization exotherm increases and moves to lower times as T_c increases up to 110 °C. From this temperature on, the crystallization peak diminishes and moves to longer times. The underlying component of the modulated heat flow is said to be equivalent to what it would be obtained in an isothermal conventional DSC measurement at the same temperature, without modulation. The time taken to develop half of the crystallization, the so-called half-time $t_{1/2}$, has been obtained through the integration of the exotherms in Fig. 2 and has been plotted in Fig. 3. $t_{1/2}$ decreases as the crystallization temperature T_c increases up to a certain temperature such that this tendency changes and the crystallization process becomes slower as T_c increases. The crystal growth rate G can be considered to be proportional to $t_{1/2}$ [13,14], and using the Lauritzen–Hoffman theory (that gives the temperature variation of G) it can be written

$$\left(\frac{1}{t_{1/2}}\right) = \left(\frac{1}{t_{1/2}}\right)_0 \exp\left[\frac{-U}{R(T_c - T_\infty)}\right] \exp\left[\frac{-K_g}{T_c(T_m - T_c)f}\right], \tag{5}$$

where $(1/t_{1/2})_0$ is a rate constant, U is an energy constant (the activation energy for segmental jump rate, in this work we adopt U = 10,450 J/mol K from [7]), T_∞ is a temperature at which all segmental motion was frozen (in this work we adopt $T_g - T_\infty$ = 30 K), f is a correction factor that takes into account the variation of the equilibrium melting enthalpy with temperature, T_m is the equilibrium melting temperature of the polymer (T_m = 206 °C for PLLA [25]) and K_g is a kinetic constant that depends on an integer and characterizes the crystallization regime. Fig. 3 shows $\ln(1/t_{1/2}) + U/R(T_c - T_\infty)$ versus $1/T_c(T_m - T_c)f$. The change in the slope at 118 °C suggest a transition from regime II (T > 118 °C) to regime III (T < 118 °C) since the Lauritzen–Hoffman theory predicts the ratio of the slopes (K_g) in the II–III transition to be equal to 2. The temperature of the transition found by means of TMDSC agrees with that previously obtained by conventional DSC [7] and optical microscopy [26]. Transition from regime II to III is related to the fact that secondary nucleation controls the linear crystal growth rate. Whereas regime II is characterized

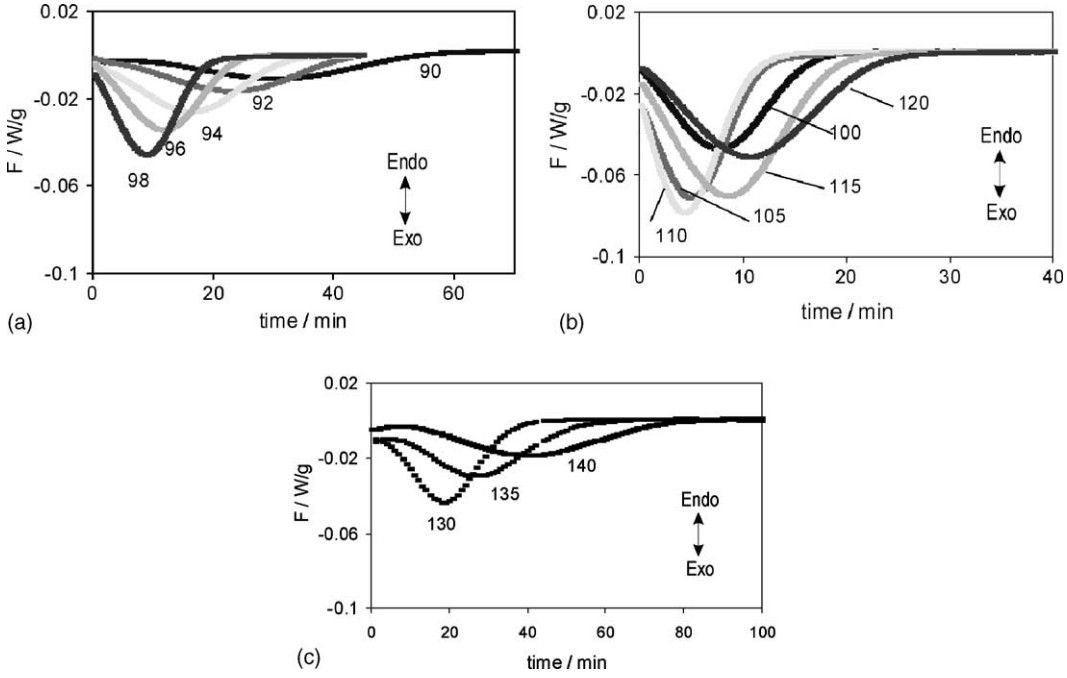

Fig. 2. Average heat flow of transformation obtained at each quasi-isothermal stage at T_c (temperature of crystallization in °C is shown next to each curve).

by multiple secondary nucleation process, in regime III, at lower temperatures, growth takes place by prolific multiple nucleation and consequently a faster crystallization process.

Besides, TMDSC provides complementary information from the same set of quasi-isothermal measurements through its characteristic magnitudes. Toda et al. model [15,16] allows to calculate the dependence of spherulite growth rate on crystallization temperature. Let the sample temperature of the quasi-isothermal stage be

$$T_s(t) = T_c + T_a\, e^{i\omega t}. \tag{6}$$

The total heat flow to the sample $\dot{Q}$ can be written to be

$$\dot{Q} = mc_p \frac{dT_s}{dT} + F(t), \tag{7}$$

where $F(t)$ is the part of the heat flow that is not inverted in rising the temperature of the system but in the phase transformation process. $F(t)$ can be thought to be the linear superposition of the heat flux of the isothermal process at T_c, $\bar{F}(t, T_c)$ that would be obtained in a conventional DSC analysis, and that due to the modulated temperature, i.e., in a formal way it could be said that $F(t)$ can be expanded about the crystallization temperature for a small temperature modulation T_a,

$$F(t, T_s) = \bar{F}(t, T_c) + \frac{dF}{dT}(t, T_c) T_a\, e^{i\omega t}. \tag{8}$$

Inserting Eq. (8) into Eq. (7), results in the above-mentioned linear superposition of heat flow responses

$$\dot{Q} = \bar{F}(t, T_c) + \left(mc_p - \frac{i}{\omega}\frac{dF}{dT} \right) \frac{dT_s}{dt}. \tag{9}$$

From the coefficient of the temperature time derivative, the complex heat capacity is defined

$$C^* = mc_p + \frac{i}{\omega}\frac{dF}{dT}. \tag{10}$$

Toda et al. assume that the real part of C^* is frequency independent for an isothermal crystallization process and the imaginary part is identified as

$$C'' = \frac{1}{\omega}\frac{dF}{dT}. \tag{11}$$

The model relates the exothermic crystallization heat flow F to the total area of growth face S_t and the crystal growth rate G,

$$F = \Delta h S_t G, \tag{12}$$

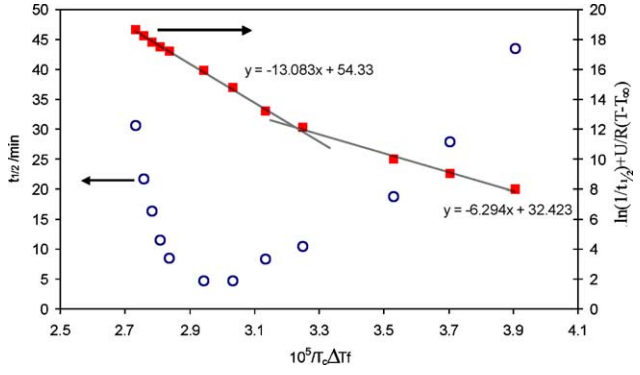

Fig. 3. Temperature dependence of $t_{1/2}$ and crystallization regime analysis based on the Lauritzen–Hoffman theory (Eq. (5) in the text).

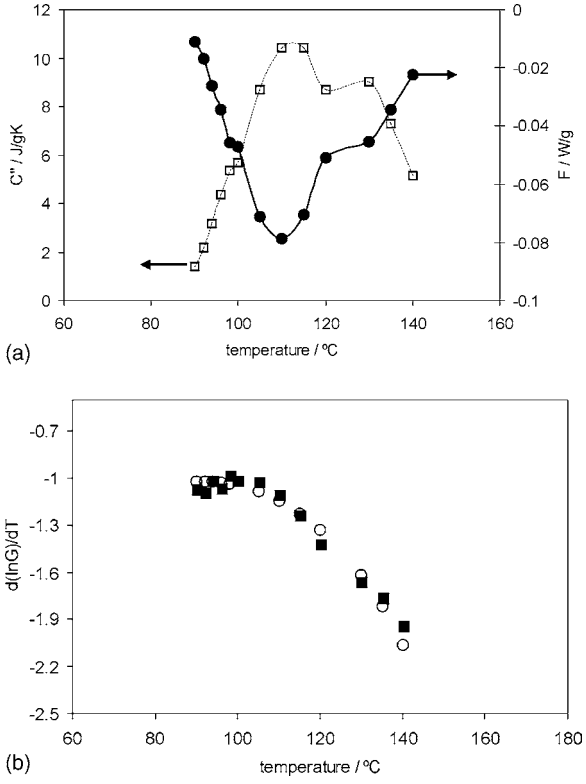

Fig. 4. (a) Temperature dependence of the imaginary part of the complex heat capacity and the exothermal crystallization heat flow (line is a guide to eye). (b) Temperature dependence of the crystal growth rate determined by Eq. (14) (■) and by the temperature derivative of Eq. (5) (◯) (with the parameters used in the fitting shown in Fig. 3).

here Δh is the change in enthalpy per unit volume. Assuming that S_t is irrelevant to temperature modulation, the temperature dependence of F is determined by the temperature dependence of the crystal growth rate

$$\frac{1}{F}\frac{dF}{dT} = \frac{1}{G}\frac{dG}{dT}, \tag{13}$$

and the temperature dependence of G is related to the modulated experiments

$$\frac{d\ln G}{dT} = \frac{-\omega C''}{F}. \tag{14}$$

Fig. 4a shows the experimental imaginary part of the complex heat capacity and the minimum F obtained at each crystallization temperature T_c. Using Eq. (14), the temperature dependence of $\ln G$ is calculated and depicted in Fig. 4b (note that Eq. (14) predicts, for a fixed T_c, a time dependent $d\ln G/dT$. It has been checked that this magnitude is almost constant for the time interval around the minimum of the exothermic crystallization event [15,16]). Two different crystal growth regimes are obtained that can be related to the Lauritzen–Hoffman regimes shown in Fig. 3. At temperatures below 110 °C, the values of $d\ln G/dT$ are almost constant, what means $\ln G \sim -kT$, and suggests an exponential dependence on the crystal growth rate on temperature, $G \sim e^{-T}$. At higher temperatures the $d\ln G/dT$ evolution is almost linear, i.e. $\ln G \sim -kT^2$, what makes $G \sim e^{-T^2}$. The temperature dependence of G is difficult to grasp from conventional DSC, however, in the way sketched a direct estimation is obtained with the supplementary information provided by modulated calorimetry. Nevertheless, the temperature dependence of $d\ln G/dT$ can be calculated from the derivative of $(1/t_{1/2})$ in terms of temperature by using Eq. (5) with the parameters obtained from the fitting of $(1/t_{1/2})$ in Fig. 3. The result has been included in Fig. 4b. It is noteworthy the good agreement between the values obtained from both methods.

Melting of polymer crystals on heating is an irreversible phenomenon usually much more complicated than crystallization due to the reorganization and recrystallization events superimposed to the melting itself during the heating scan. It is known that the complex heat capacity in a modulated scan with non-zero average heating rate shows a strong frequency dependence both in the real and imaginary part of the complex heat capacity that is ascribed to the time scale coincidence of the characteristic time of the melting process and the period of the modulated temperature [9,18,19]. Fig. 5 shows results on heating with four different modulation periods. The heating rate dependent heat capacity C_β (shown in Fig. 5a) is equivalent to that of a conventional DSC measurement. The four curves corresponding to the four modulation periods used in this work are superimposed showing, as expected, no frequency dependence. The endothermic melting peak seems to be the superposition of two different ones. Whether these peaks corresponds either to two different crystals morphologies due to the existence of a transition from one kinetic crystallization regime to other around 118 °C or to a superimposed exothermal event due to recrystallizations and reorganizations once the melting process starts is not discussed here. It is not under question that both peaks show the corresponding ones in the modulated experiments and that both of them are frequency dependent (what on the other hand supports the hypothesis of two different crystal morphologies since it is known the frequency independence of the exothermal process on heating [19,27]). The magnitude of the complex heat capacity is shown in Fig. 5b. A strong frequency dependence is found, and the magnitude of the peak decreases as frequency increases. From the magnitude of C^* and the phase lag φ, the real and imaginary parts of the complex heat capacity are calculated (Eqs. (2a) and (2b)) and results are shown in Fig. 5c and d, respectively. Both of them show strong frequency dependence with the same tendency as the magnitude of the complex heat capacity. It is interesting to note that both C' and C'' have similar values, indicating the high values of the phase lag φ (above 40°). The analysis of the frequency dependence of C' and C'' at different temperatures can provide information about the kinetics of the melting process through the extended model of Toda et al. to the melting phenomenon [19]. Let the heat flow $F(t)$ be expanded about the average sample temperature $\overline{T}_s$, i.e. about the temperature that the equivalent DSC scan would have at that time. The same Eq. (8) would be obtained but in terms of $\overline{T}_s$ instead of T_c in which $\overline{F}$ represents now the heat flow

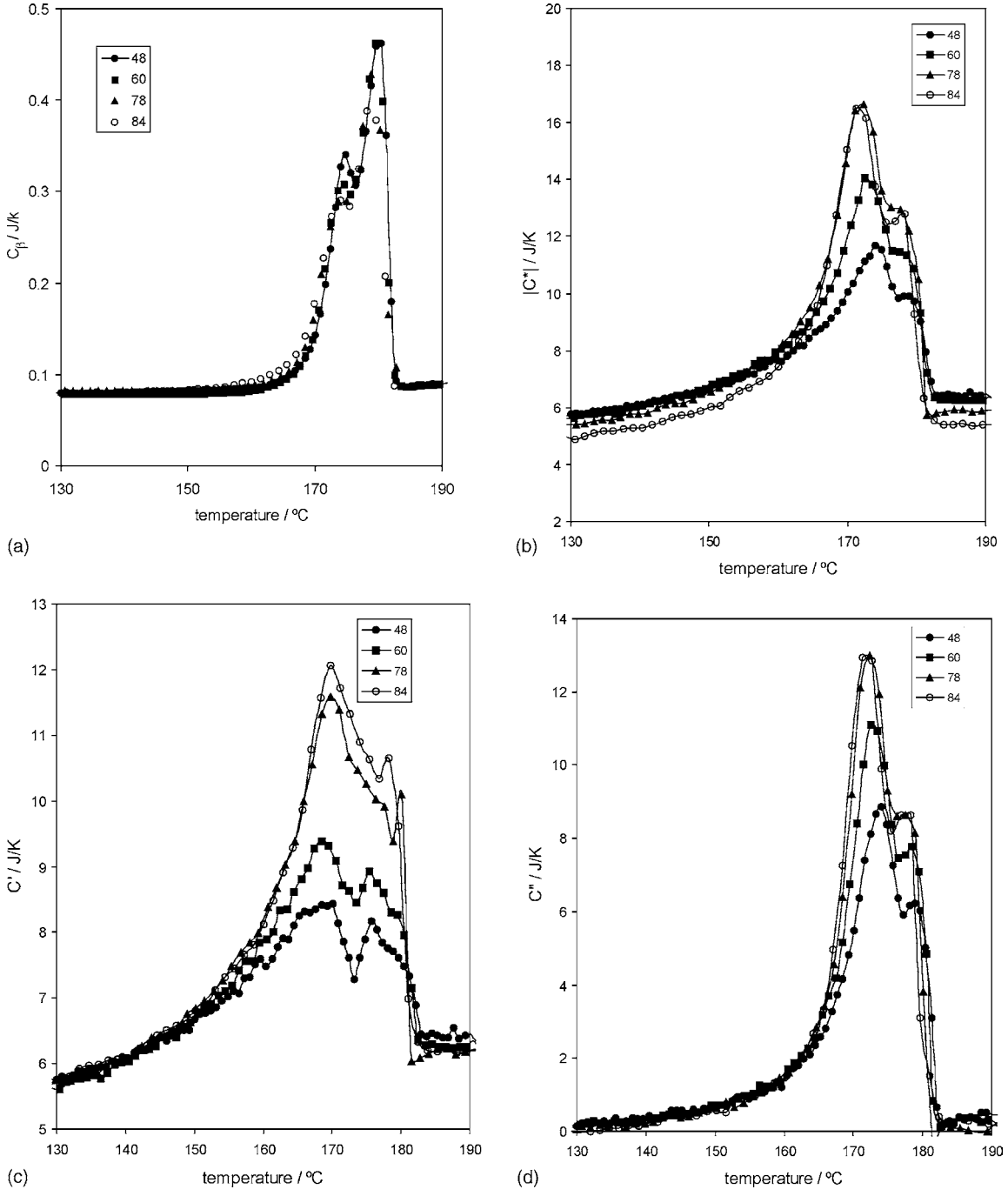

Fig. 5. Results of TMDSC with four modulation periods vs. temperature. (a) Underlying heat capacity, C_β. (b) Magnitude of the complex heat capacity. Real (c) and imaginary (d) parts of the complex heat capacity.

of the phase transformation, i.e. that that would be obtained in a conventional DSC analysis at the average heating rate.

Let $\phi(t, T_m)\,dT_m$ be the fraction of crystallites having, at time t, the melting temperature in the range from T_m to $T_m + dT_m$. The endothermic heat flow of melting can be expressed as

$$F = \Delta H \frac{d}{dt} \int_0^\infty \phi(t, T_m)\,dT_m, \tag{15}$$

where ΔH is the total enthalpy change of the system on melting. The model assumes that the evolution in time of $\phi(t, T_m)$ is controlled by a melting rate coefficient, R, that is a function of superheating, $\Delta T = T_s - T_m$:

$$\frac{d\phi(t, T_m)}{dt} = -R(\Delta T)\phi(t, T_m) \tag{16}$$

Solving this equation, with a concrete expression for the superheating dependence of R, allows obtaining via Eq. (15) an

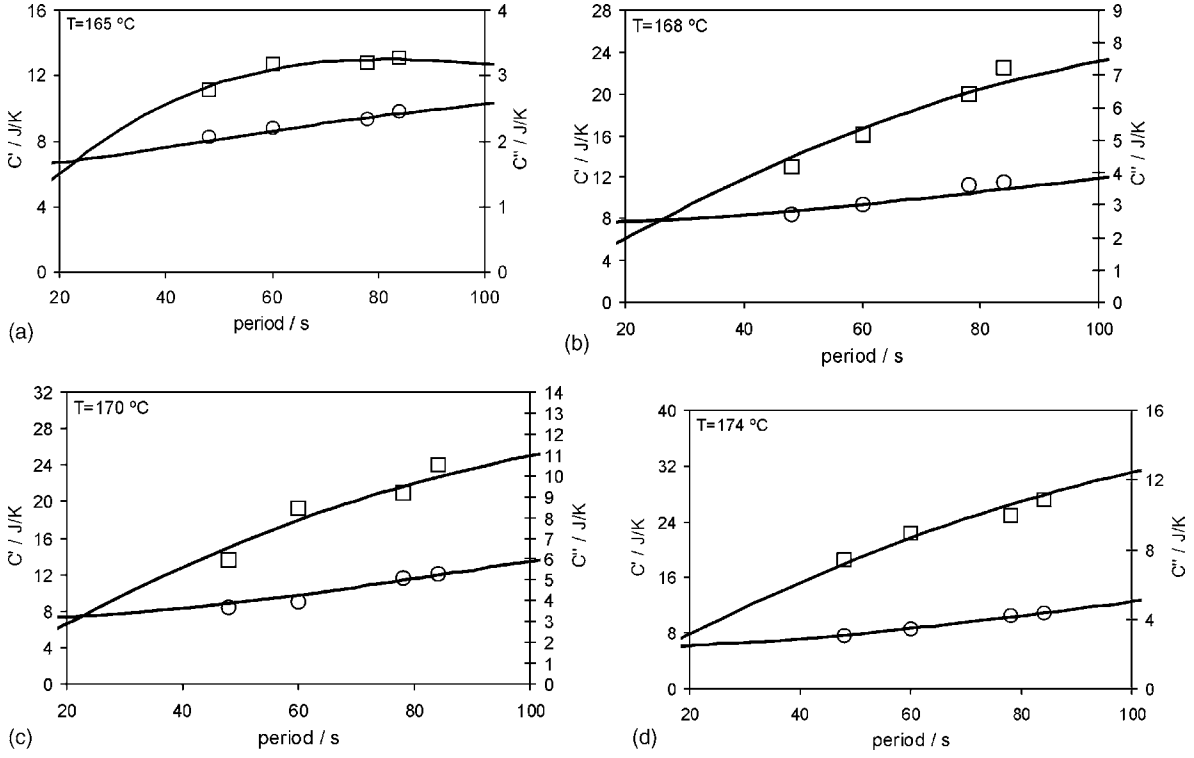

Fig. 6. Real (□) and imaginary (◯) parts of the complex heat capacity vs. the modulation period at four different temperatures. The continuous line corresponds to Eq. (21) with the adjustable parameters (c_p, ϕ_0, τ_2).

expression for the heat flow of transformation, which can be related to the complex heat capacity through its first harmonic in the Fourier expansion.

Since the heating run satisfies the condition of heating always (Eq. (3)), crystallization cannot be due to temperature drops during the modulated heating scan. Besides, the model does not consider the presence of recrystallization or reorganization of the crystallites. Under these conditions Eq. (16) can be applied, and its solution is

$$\phi(t, T_\mathrm{m}) = \phi_0 \exp\left[-\int_0^t R\,\mathrm{d}t'\right], \tag{17}$$

where ϕ_0 is the initial distribution of crystallite fractions that is assumed to be uniform. On this basis, considering the linear expansion of the melting rate coefficient, R, for small temperature modulation, $\mathrm{d}F/\mathrm{d}T$ is calculated introducing the expression obtained via Eq. (17) for $\phi(t, T_\mathrm{m})$ through the expanded R into Eq. (15) and considering the first harmonic of its Fourier series. In this way one obtains [18–21]

$$C^* = mc_p + \frac{\mathrm{i}}{\omega}\frac{\mathrm{d}F}{\mathrm{d}T}(\omega). \tag{18}$$

that is formally Eq. (10) but where the frequency dependence of $\mathrm{d}F/\mathrm{d}T$ is assumed trying to account for the experimental facts. That is, now is

$$\frac{\mathrm{d}F}{\mathrm{d}T}(\omega) = \frac{\omega}{\mathrm{i}}\Delta H\phi_0\beta\int_0^\infty \mathrm{e}^{-\mathrm{i}\omega x} \times\left[\mathrm{e}^{-\int_0^x R(\beta y)\,\mathrm{d}y}\int_0^x R'(\beta y)\,\mathrm{e}^{\mathrm{i}\omega y}\,\mathrm{d}y\right]\mathrm{d}x. \tag{19}$$

Depending on the superheating dependence of the melting rate coefficient, the kinetic response will change. Following Toda et al. [18–21] three different expressions have been tested. The first of them is the case of a constant rate coefficient, independent of superheating ($R = R_0$), the second one is a linear dependence of the melting rate on superheating ($R = a\Delta T$), and the third one is an exponential dependence ($R = (a/c)(\mathrm{e}^{c\Delta T} - 1)$). The last one is the most general of the three and includes the other two as special cases. Introducing the exponential dependence in Eq. (19), the following expression is obtained:

$$\frac{\mathrm{d}F}{\mathrm{d}T}(\omega) = \frac{\omega}{\mathrm{i}}\frac{\Delta H\phi_0}{1+\mathrm{i}\omega\tau_2}\frac{1}{\tau_3}\int_0^\infty (\mathrm{e}^{x/\tau_2} - \mathrm{e}^{-\mathrm{i}\omega x}) \times\exp\left[-\frac{\tau_2}{\tau_3}\left(\mathrm{e}^{x/\tau_2} - 1 - \frac{x}{\tau_2}\right)\right]\mathrm{d}x, \tag{20}$$

where

$$\tau_2 = \frac{1}{\beta c}, \qquad \tau_3 = \frac{c}{a}.$$

It must be here remarked that in Refs. [18,19] this equation is printed with a mistake.

It is easy to show that when $\tau_2 \gg \tau_3$ the frequency response corresponds to a linear dependence of the melting coefficient on superheating, and that it corresponds to a constant value of R in the case when $\tau_3 \gg \tau_2$. Fig. 6 shows the frequency dependence of the real and imaginary parts of the complex heat capacity obtained at several temperatures. The fit was adequate with the time parameters such that $\tau_3 \gg \tau_2$, i.e., what corresponds to a time independence melting rate coefficient,

$$\frac{\mathrm{d}F}{\mathrm{d}T}(\omega) \approx \frac{\omega}{\mathrm{i}} \frac{\Delta H \phi_0}{1 + \mathrm{i}\omega\tau_2}. \tag{21}$$

Fitting an expression for $\mathrm{d}F/\mathrm{d}T(\omega)$ to the experimental results implies to find a set of parameters (c_p, ϕ_0, τ) that reproduces, at the same time, and for a fixed temperature, the real and imaginary kinetic response of the material. The fit was adequate with Eq. (21) in the whole temperature range of the melting process. This dependence seems to suggest that the heating rate dependence of the characteristic time is $\tau \propto \beta^{-1}$ in the whole temperature range. Nevertheless, there is only a small difference between the frequency response function of Debye's type (Eq. (21)) and the one that accounts for a linear dependence of R on superheating, that predicts the heating rate dependence of the characteristic time to be $\tau \propto \beta^{-1/2}$ [18–21]. Therefore, it is quite difficult to differentiate the frequency dependence experimentally obtained by TMDSC: the exponent x of $\tau \propto \beta^{-x}$ can be between 0.5 and 1.

The model needs the linear response of the system to the modulated temperature profile. At least two independent facts must be checked: linearity and steady-state condition in the melting region. On the one hand the oscillation temperature is not a pure sinusoidal but a saw-tooth modulation. However, for the experimental conditions chosen in this work, the apparatus rounds the cups of the programmed wave form, and the temperature profile to which the sample is finally subjected is quite similar to a pure sinusoidal: Fig. 7a shows the Fourier analysis of the temperature cycle and the negligible presence of higher harmonics. Fig. 7b shows that the melting phenomenon takes place in the linear regime: the response (heat flow) is such that the highest component is due to fundamental frequency and much lower for higher harmonics. On the other hand, steady-state condition have to be checked for the application of the model: Lissajous diagrams of the modulated heat flow against the modulated sample temperature showing several cycles in the melting area are shown in Fig. 8; a closed loop can be observed in all cases.

Until know the kinetics of melting and crystallization has been discussed as a first order irreversible transition; once a molecule is completely melted, reversibility is lost due to the need for molecular nucleation and the need of overcome a free energy barrier [28]. However, the development of TMDSC allows to study what it is called the 'reversing' heat capacity of the material, in the sense that the thermal response is recovered in one period of the thermal modulation [9,20]: the

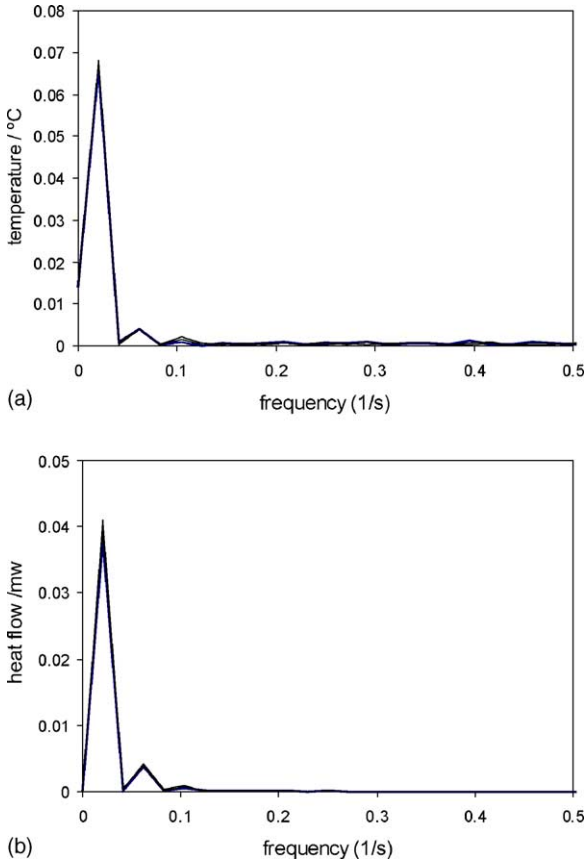

Fig. 7. Magnitude of the spectral analysis of the modulated (a) temperature and (b) heat flow. The almost coincident different lines correspond to different cycles of the modulated scan in the melting region.

polymer molecules partially melted in one cycle are still attached to crystals that melt at a higher temperature and can serve as molecular nuclei. The reversing heat capacity is just the magnitude of the previously defined complex heat capacity (Eq. (1)) and its permanent presence (i.e., non-relaxing to zero behaviour for long enough times) in the case of an oscillating temperature superimposed to an isothermal stage was explained as an indication of the recrystallization behaviour in the melting process. The magnitude of the complex heat capacity for a quasi-isothermal temperature program is shown in Fig. 9. The material shows a negligible reversing heat capacity in slow cooling ($C_{p\mathrm{max}}/C_{p\mathrm{melt}} \sim 1$) and a small one in the melting range, on heating after fast cooling ($C_{p\mathrm{max}}/C_{p\mathrm{melt}} \sim 1.15$). This effect has been correlated to the ability of sliding diffusion of the polymer chains in the crystals [22] and our results suggest that there is little sliding diffusion due, maybe, to the steric hindrance of the methyl side group. The absence of reversing heat capacity on slow cooling is related to the need of a high supercooling for crystallization to start, as in fact happens in PLLA [7]. A deeper insight in the reversible melting process is being gained in this polymer by a more detailed experimental procedure (influence of the temperature step, temperature amplitude, time relaxation of the reversing heat capacity and its

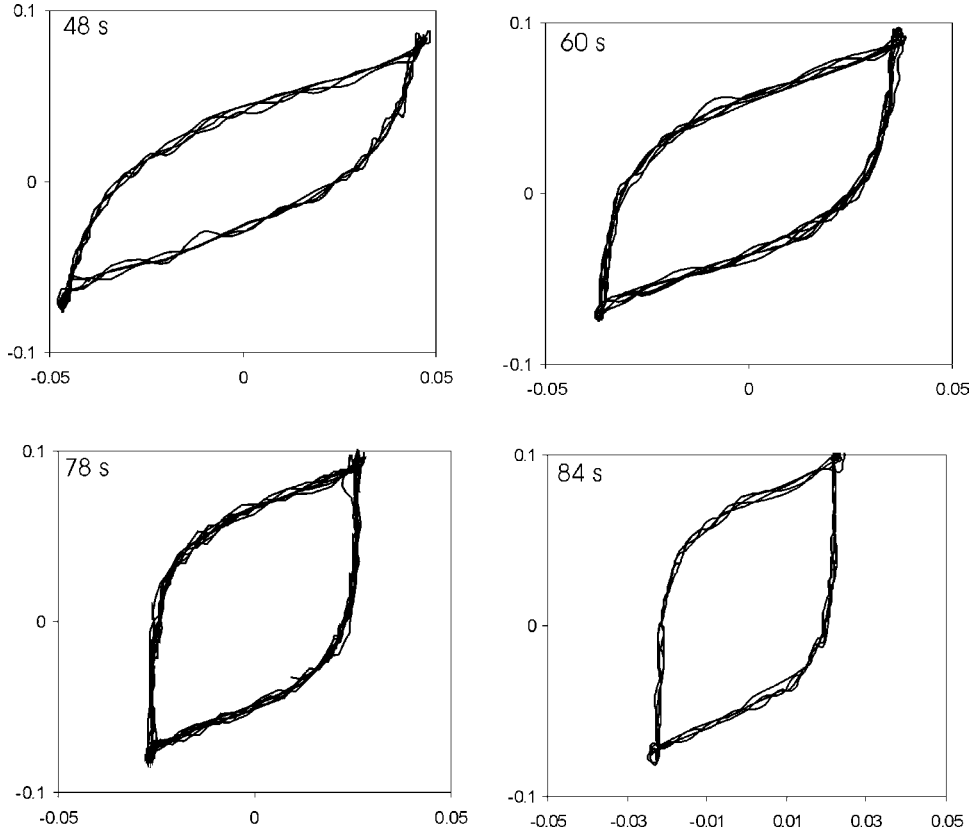

Fig. 8. Lissajous diagrams of several cycles of the modulated component of the heat flow vs. the modulated component of the temperature calculated at the high temperature melting region. The average heating rate was 1.5 °C/min, the period is indicated in each diagram.

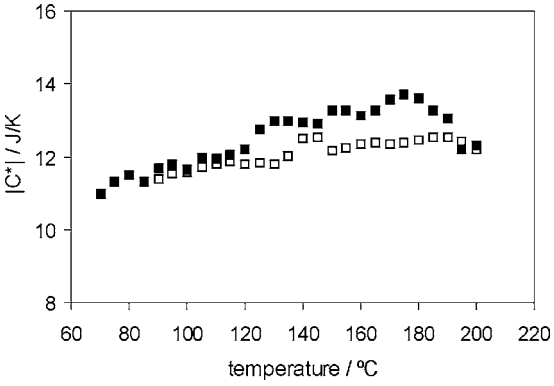

Fig. 9. Quasi-isothermal TMDSC measurement: (□) slow cooling process, (■) heating after fast cooling.

modelling, steady-state conditions, different thermal histories before step modulation) [29].

4. Conclusions

TMDSC is an analytical tool that can supply valuable information about the kinetics of melting and crystallization of a biodegradable polylactide. Quasi-isothermal crystallization shows via the Lauritzen–Hoffman theory the existence of a change in the crystallization regime around 118 °C that is confirmed by the modulated experiments from where a direct estimation of the crystallization rate is obtained. The kinetic modelling of the melting process suggests the exponential dependence of the melting rate coefficient on superheating. Finally, an introduction to the reversible crystallization and melting of PLLA is done. This biodegradable polymer shows a low reversing contribution to the heat capacity on heating that is almost negligible on cooling. A further research of this phenomenon in PLLA is in progress.

Acknowledgements

The authors thank Kadriye Tuzlakoglu for providing the PLLA used in this work. MSS and JLGR acknowledge the support of CICYT through the MAT 2001-2678-C02-01 project and the support to their research group by the Generalitat Valenciana through the Gupos03/018 project. JFM acknowledges the financial support from FCT, through the POCTI and FEDER programmes.

References

[1] A. Södegard, M. Stolt, Prog. Polym. Sci. 27 (2002) 1123.
[2] R.C. Thomson, M.C. Wake, M.J. Yaszemski, A.G. Mikos, Adv. Polym. Sci. 122 (1995) 245.

[3] H.D. Kim, E.H. Bae, I.C. Kwon, R.R. Pal, J.D. Nam, D.S. Lee, Biomaterials 25 (2004) 2319.
[4] M. Reeve, S. McCarthy, M. Downey, R. Gross, Macromolecules 27 (1994) 825.
[5] R. MacDOnald, S. McCarthy, R. Gross, Macromolecules 29 (1996) 7356.
[6] H. Tsuji, Y. Ikada, Polymer 36 (1995) 2709.
[7] S. Iannace, A. Maffezzoli, G. Leo, J. Nicolais, Polymer 42 (2001) 3799.
[8] R. Vasoille, J. Pérez, Ann. Phys. Fr. 10 (1985) 10.
[9] B. Wunderlich, Prog. Polym. Sci. 28 (2003) 383.
[10] J.E.K. Schawe, Thermochim. Acta 261 (1995) 183.
[11] J.E.K. Schawe, Thermochim. Acta 305 (1997) 111.
[12] J.E.K. Schawe, G.W.H. Höhne, Thermochim. Acta 287 (1996) 213.
[13] J.D. Hoffman, G.T. Davis, J.I. Lauritzen, Treatise on Solid State Chemistry: Crystalline and Non-crystalline Solids, Plenum Press, New York, 1976.
[14] J.D. Hoffman, Polymer 24 (1983) 3.
[15] A. Toda, T. Oda, M. Hikosaka, Y. Saruyama, Polymer 38 (1997) 2849.
[16] A. Toda, T. Oda, M. Hikosaka, Y. Saruyama, Polymer 38 (1997) 231.
[17] B. Wunderlich, Macromolecular Physics, vol. 3, Academic Press, New York, 1976.
[18] A. Toda, C.C. Tomita, M. Hikosaka, Y. Saruyama, J. Therm. Anal. Cal. 64 (2001) 775.
[19] A. Toda, C.C. Tomita, M. Hikosaka, Y. Saruyama, Polymer 39 (1998) 5093.
[20] A. Toda, T. Arita, C. Tomita, M. Hikosaka, Thermochim. Acta 330 (1999) 75.
[21] A. Toda, Y. Saruyama, Polymer 42 (2001) 4727.
[22] W. Hu, T. Albrecht, G. Strobl, Macromolecules 32 (1999) 7548.
[23] R. Scherrenberg, V. Mathot, A. Van Hemelrijck, Thermochim. Acta 330 (1999) 3.
[24] H. Yavuz, C. Babac, K. Tuzlakoglu, E. Piskin, Polym. Degrad. Stabil. 75 (2002) 431.
[25] R. Vasanthakurami, A.J. Pennings, Polymer 24 (1983) 175.
[26] M.L. Di Lorenzo, Polymer 42 (2001) 42.
[27] M. Salmerón Sánchez, M. Monleón Pradas, J.L. Gómez Ribelles, Polymer 42 (2002) 6273.
[28] I. Okazaki, B. Wunderlich, Macromolecules 30 (1997) 1758.
[29] M. Salmerón Sánchez, J.L. Gómez Ribelles, J.F. Mano, in preparation.